Materials Research Proceedings 43 (2024) 246-253 https://doi.org/10.21741/9781644903216-32

Sliding mode control for grid integration of point absorber type wave energy converter

Abdin Y. ELAMIN[1,a] and Addy WAHYUDIE[1,b*]

[1]Department of Electrical and Communication Engineering, United Arab Emirates University (UAEU), Al Ain, United Arab Emirates

[a]201890100@uaeu.ac.ae, [b]addy.w@uaeu.ac.ae

Keywords: Current Controllers, DC Bus Regulation, Grid Integration, Phase Locked Loop Point Absorber, Resistive Loading, Sliding Mode Control, Wave Energy

Abstract. This paper addresses the integration of a point absorber type wave energy converter into power grids, a process complicated by wave energy's intermittent and unpredictable nature. It proposes a sliding mode control strategy with an exponential reaching law in a voltage-oriented control architecture for the grid-side converter of the point absorber. The control objective is to maximize the transfer of generated power to the electrical grid, while concurrently stabilizing the DC bus voltage at a predetermined value and achieving a unity power factor. Results from simulations conducted within a MATLAB framework underscore the efficacy of the sliding mode control approach in sustaining specified DC bus voltage values, and in regulating the direct and quadrature currents by minimizing their respective tracking errors.

Introduction

Wave energy has a potential of 0.534 to 17.5 PWh/year and offers a high energy density with minimal environmental impact [1]. Its availability rate of up to 90% is significantly greater than the 20%-30% of solar and wind energies [2-3]. Wave energy converters (WECs), including various types such as point absorbers (PAs), are used to transform wave energy into electricity. Despite its benefits, wave energy's integration into power grids faces challenges due to its intermittent and unpredictable nature, causing fluctuations in power output that lack synchronization with key grid parameters, such as voltage, phase angle, and frequency. Asynchronization can significantly degrade grid stability and may introduce unwanted effects such as harmonics, frequency deviation and voltage collapse. The criticality of this issue escalates when the grid faces disturbances and unbalanced faults. The back to back converter topology is particularly effective for ensuring the poor power quality of the WEC doesn't propagate into the grid.

The role of the machine-side converter (MSC), i.e., AC/DC converter, is to maximize wave energy extraction, while the grid-side converter (GSC), i.e., DC/AC converter, is tasked with ensuring the synchronization of a constant voltage and frequency to the grid. In terms of GSC control strategies, Proportional-Integral (PI) controllers have been popularly suggested for regulating DC bus voltage and ensuring unity power factor by synchronizing current waveforms with the grid's frequency [4]. However, their performance is constrained by their reliance on linear models and sensitivity to parameter variations. Given the strongly coupled and nonlinear nature of the GSC system, a nonlinear control strategy could potentially enhance both static and dynamic performance. A study in [5] proposed a Lyapunov-based nonlinear controller for active power regulation and zero reactive power injection into the grid.

Sliding mode control (SMC) techniques have be used extensively as nonlinear controllers in GSCs for wind energy and photovoltaic applications [6], yet they haven't been implemented in WEC systems. Their robustness to parameter variations and disturbances [7], make them prime candidates in grid tied WEC applications. This paper proposes a SMC strategy for a GSC in a PA,

utilizing a voltage-oriented control (VOC) architecture. The VOC incorporates two cascaded control loops, with the outer-loop focusing on DC bus voltage regulation. The inner-loop ensures that the GSC output currents accurately track the reference currents from the upper-loop and are synchronized with the grid frequency. A phase-locked-loop (PLL) is adopted for grid synchronization. The resistive loading control employed by the MSC for maximum wave energy absorption is not discussed in this paper, with a comprehensive explanation available in [8]. The paper is organized in the following manner: Initially, it provides a comprehensive model of the PA system from wave to grid. Subsequently, it delves into the design aspects of the GSC control strategy. This is followed by an analysis of simulation results. Finally, the paper ends with a conclusion.

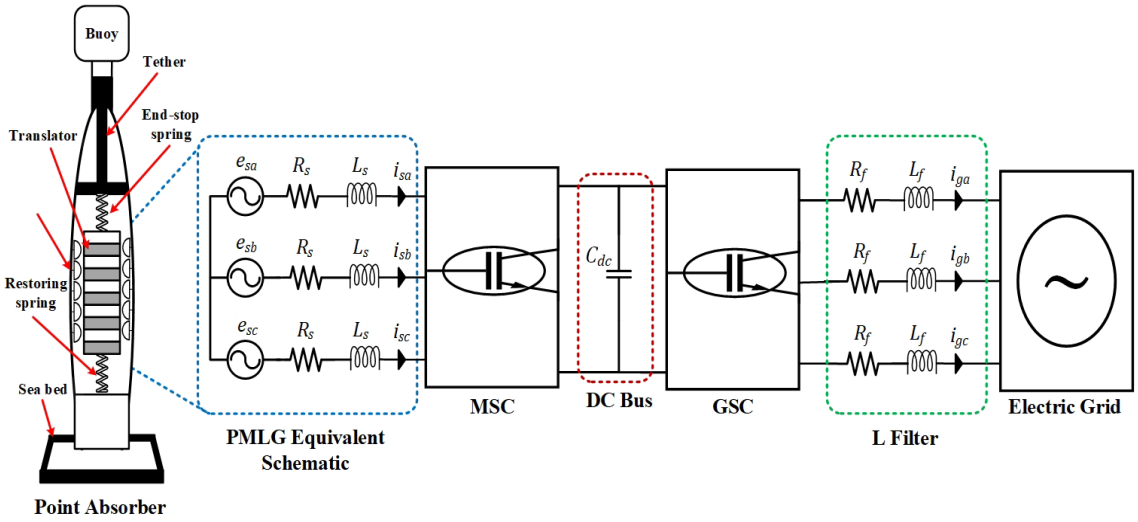

Figure 1: Point absorber system schematic.

System Model

A visual description of the PA system is shown in Fig.1. The PA consists of a floating cylindrical buoy, tethered to a three-phase permanent magnet linear generator (PMLG). A back-to-back converter topology, linking the MSC and GSC via a DC bus, serves as the intermediary between the PA and the electrical grid. Finally, an L filter is used to mitigate the harmonics distortion in the GSCs' output. This topology offers the ability to decouple the PA from the grid, enabling the system model to be split into two independent subsystems: the machine-side and the grid-side.

Machine-side Model

The machines-side model incorporates the wave-buoy hydrodynamic interaction and the electrical dynamics of the PMLG. By assuming only linear forces, the buoy heaving motion during wave interaction can be formulated using Newton's second law of motion given by

$$M\ddot{z}(t) = f_{ex}(t) - f_r(t) - f_b(t) - f_{rs}(t) + f_u(t). \quad (1)$$

where M being the buoy mass, and $\ddot{z}(t)$ is the heave acceleration. $f_{ex}(t)$ corresponds to the wave excitation force, $f_r(t)$ to the radiation force, $f_b(t)$ to the hydrostatic buoyancy force, $f_{rs}(t)$ to the restoring spring force, and $f_u(t)$ to the electromagnetic control force exerted by the PMLG.

The translator in the PMLG is mechanically linked to the buoy, thereby mirroring its heave motion. Consequently, this translator movement induces electromotive force (EMF) voltages in the stationary windings of the PMLG. The PMLG model in the abc frame is given as

$$\boldsymbol{e_s}(t) = R_s\boldsymbol{i_s}(t) + j\omega_e(t)L_s\boldsymbol{i_s}(t) + \boldsymbol{v_s}(t). \quad (2)$$

where $\boldsymbol{e_s}(t) = [e_{sa}(t) \quad e_{sb}(t) \quad e_{sc}(t)]^T$, $\boldsymbol{i_s}(t) = [i_{sa}(t) \quad i_{sb}(t) \quad i_{sc}(t)]^T$, R_s, L_s and $\boldsymbol{v_s}(t) = [v_{sa}(t) \quad v_{sb}(t) \quad v_{sc}(t)]^T$ are the three phase EMF voltage, stator currents, stator resistance, stator inductance and the three phase voltage terminals. The resistance and inductance represent the internal losses of the generator due to the copper windings and the magnetic field, respectively. By applying Parke transformation to Eq. 2 and including the MSC switching inputs, the machine-side model can be expressed in the synchronous reference (d-q) frame as

$$\frac{di_{sd}(t)}{dt} = \frac{-R_s i_{sd}(t)}{L_s} + \omega_e(t) i_{sq}(t) - \frac{u_{sd}(t)}{L_s}. \tag{3}$$

$$\frac{di_{sq}(t)}{dt} = \frac{-R_s i_{sq}(t)}{L_s} - \omega_e(t) i_{sd}(t) - \frac{\omega_e(t)}{L_s}\varphi_{pm} - \frac{u_{sq}(t)}{L_s}. \tag{4}$$

where $i_{sd}(t)$ and $i_{sq}(t)$ are the direct and quadrature components of the stator current, whereas $u_{sd}(t)$ and $u_{sq}(t)$ are the *d-q* components of MSC switching signals. The flux linkage is denoted by φ_{pm} and the angular frequency $\omega_e(t)$ is obtained as follows

$$\omega_e(t) = \frac{\pi}{\tau_p}\dot{z}(t). \tag{5}$$

with $\dot{z}(t)$ and τ_p being the heave velocity and the PMLG pole pitch, respectively. The captured wave power $P_m(t)$ and PA generated electrical power $P_e(t)$ are given by

$$P_m(t) = f_u(t)\, \dot{z}(t) \; = \frac{3\pi\varphi_{pm}}{2\tau_p} i_{sq}(t)\dot{z}(t). \tag{6}$$

$$P_e(t) = \frac{3}{2}\big(v_{sd}(t) i_{sd}(t) + v_{sq}(t)\, i_{sq}(t)\big) = v_{dc}(t)\, i_{dc}(t). \tag{7}$$

with $v_{dc}(t)$ and $i_{dc}(t)$ being DC bus voltage and DC current output of the MSC, respectively.

Grid-side Model

The grid-side model includes the GSC, L filter and electric grid. The grid is modeled as a voltage source in series with an impedance based on its Thevenin equivalent circuit. The impedance consists of a resistor R_g and inductance L_g to account for transmission line and power transformer effects. The grid-side model can be written using Kirchhoff's laws as follows

$$\boldsymbol{v_g}(t) = \big(R_f + R_g\big)\boldsymbol{i_g}(t) + \big(L_f + L_g\big)\frac{d\boldsymbol{i_g}(t)}{dt} + \boldsymbol{e_g}(t). \tag{8}$$

where $\boldsymbol{e_g}(t) = [e_{ga}(t) \quad e_{gb}(t) \quad e_{gc}(t)]^T$, $\boldsymbol{i_g}(t) = [i_{ga}(t) \quad i_{gb}(t) \quad i_{gc}(t)]^T$ and $\boldsymbol{v_g}(t) = [v_{ga}(t) \quad v_{gb}(t) \quad v_{gc}(t)]^T$ are the three phase grid voltages, grid currents and GSC voltage output, respectively. R_f represents a small resistor to account for losses in the filter. By applying Parke transformation to Eq. 8, the grid-side model in the (*d-q*) frame at grid voltage frequency ω_g is given by

$$\frac{di_{gd}(t)}{dt} = \frac{-\big(R_f+R_g\big)i_{gd}(t)}{\big(L_f+L_g\big)} - \frac{e_{gd}(t)}{\big(L_f+L_g\big)} + \frac{u_{gd}(t)}{\big(L_f+L_g\big)} + \omega_g(t) i_{gq}(t). \tag{9}$$

$$\frac{di_{gq}(t)}{dt} = \frac{-\big(R_f+R_g\big)i_{gq}(t)}{\big(L_f+L_g\big)} - \frac{e_{gq}(t)}{\big(L_f+L_g\big)} + \frac{u_{gq}(t)}{\big(L_f+L_g\big)} - \omega_g(t) i_{gd}(t). \tag{10}$$

here, $i_{gd}(t)$, $i_{gq}(t)$, $e_{gd}(t)$, $e_{gq}(t)$, $u_{gd}(t)$ and $u_{gd}(t)$ are the *d-q* components of the grid currents, grid voltages and GSC switching signals, respectively. The active and reactive power delivered to the grid are given respectively by

$$P_g(t) = \frac{3}{2}\left(e_{gd}(t)i_{gd}(t) + e_{gq}(t)i_{gq}(t)\right). \quad (11)$$

$$Q_g(t) = \frac{3}{2}\left(e_{gq}(t)i_{gd}(t) - e_{gd}(t)i_{gq}(t)\right). \quad (12)$$

Finally, the power exchange in the DC bus can expressed as follows

$$C_{dc}\, v_{dc}(t)\frac{dv_{dc}(t)}{dt} = P_e(t) - P_g(t). \quad (13)$$

where C_{dc} represents the DC bus capacitor.

Controller Design

The objective of the SMC is to govern the GSC operations to ensure the PA output power is grid compatible in terms of frequency synchronization, while regulating the DC bus voltage. Assuming no limitations on the grid power intake, the PA operates at peak generation capacity. A schematic of the SMC strategy in a VOC architecture is illustrated in Fig. 2.

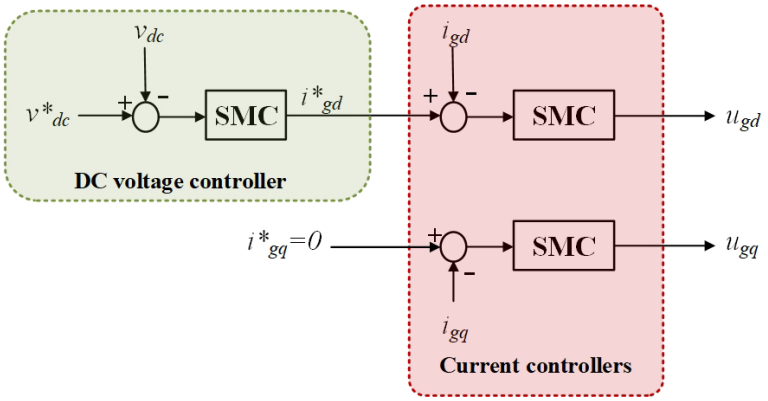

Figure 2: proposed GSC control strategy.

Outer Voltage Control Loop

As observed in Fig. 2, the voltage controller's output is the direct current reference $i^*_{gd}(t)$, which dictates the power level the GSC must either supply or absorb to keep the DC bus voltage at a fixed level. The quadrature current reference $i^*_{gq}(t)$ is set to zero to attain a unity power factor. Substituting Eq. 7 and Eq. 11 into Eq. 13, and simplifying that the quadrature grid voltage is zero $\left(e_{gq}(t) = 0\right)$, the DC voltage can be written as

$$\frac{dv_{dc}(t)}{dt} = \frac{1}{C_{dc}} i_{dc}(t) - \frac{3}{2C_{dc}v_{dc}(t)} e_{gd}(t)i_{gd}(t). \quad (14)$$

The SMC design requires formulating a sliding surface function $S_v(t)$ of the following form

$$S_v(t) = e_v(t) + \lambda_v \int e_v(t)\, dt. \quad (15)$$

here, $e_v(t)$ and λ_v are the voltage tracking error and convergence rate of $S_v(t)$. The tracking error $e_v(t)$ and its derivative are given by

$$e_v(t) = v^*_{dc}(t) - v_{dc}(t), \qquad \dot{e}_v(t) = \dot{v}^*_{dc}(t) - \dot{v}_{dc}(t). \quad (16)$$

where $v^*_{dc}(t)$ is the DC voltage reference. Based on Eq. 14, $\dot{e}_v(t)$ can be expressed as

$$\dot{e}_v(t) = \dot{v}^*_{dc}(t) - \frac{1}{C_{dc}} i_{dc}(t) + \frac{3}{2C_{dc}v_{dc}(t)} e_{gd}(t)i_{gd}(t). \quad (17)$$

By differentiating Eq. 15, yields the following

$$\dot{S}_v(t) = \dot{v}^*_{dc}(t) - \frac{1}{C_{dc}} i_{dc}(t) + \frac{3}{2C_{dc}v_{dc}(t)} e_{gd}(t) i_{gd}(t) + \lambda_v e_v(t). \quad (18)$$

Equating Eq. 18 to zero, and solving for $i_{gd}(t)$, yields the equivalent direct current reference $i^*_{gd,eq}(t)$ as follows

$$i_{gd,eq}(t) = \frac{2v_{dc}(t)}{3e_{gd}(t)} i_{dc}(t) - \frac{2C_{dc}v_{dc}(t)}{3e_{gd}(t)} \left(\dot{v}^*_{dc}(t) + \lambda_v e_v(t)\right). \quad (19)$$

Adding the exponential reaching law found in [7] to Eq. 19, gives the direct current reference $i^*_{gd}(t)$ as

$$i^*_{gd}(t) = \frac{2v_{dc}(t)}{3e_{gd}(t)} i_{dc}(t) - \frac{2C_{dc}v_{dc}(t)}{3e_{gd}(t)} \left(\dot{v}^*_{dc}(t) + \lambda_v e_v(t)\right) - \varepsilon_v \, sgn\left(S_v(t)\right) - k_v S_v(t). \quad (20)$$

with ε_v and k_v being positive tuning variables used to guarantee faster convergence speed, and the notation $sgn\left(S_v(t)\right)$ represents the signum function of $S_v(t)$.

Inner Current Control Loop

Similar to the voltage controller, the current controllers require defining the d-q current tracking errors given by

$$e_{id}(t) = i^*_{gd}(t) - i_{gd}(t), \qquad e_{iq}(t) = i^*_{gq}(t) - i_{gq}(t). \quad (21)$$

The sliding surface functions can be defined as

$$S_d(t) = e_{id}(t) + \lambda_i \int e_{id}(t)\, dt, \qquad S_q(t) = e_{iq}(t) + \lambda_i \int e_{iq}(t)\, dt. \quad (22)$$

where i^*_{gd} and i^*_{gq} represent the d-q stator current references, whereas λ_i denote the convergence rate of the sliding functions $S_d(t)$ and $S_q(t)$. The derivatives of Eq. 22 using Eq. 9, Eq. 10 and Eq. 21 is given by

$$\dot{S}_d(t) = i^*_{gd}(t) + \frac{(R_f+R_g)i_{gd}(t)}{(L_f+L_g)} + \frac{e_{gd}(t)}{(L_f+L_g)} - \frac{u_{gd}(t)}{(L_f+L_g)} - \omega_g(t) i_{gq}(t) + \lambda_i e_{id}(t). \quad (23)$$

$$\dot{S}_q(t) = i^*_{gq}(t) + \frac{(R_f+R_g)i_{gq}(t)}{(L_f+L_g)} + \frac{e_{gq}(t)}{(L_f+L_g)} - \frac{u_{gq}(t)}{(L_f+L_g)} + \omega_g(t) i_{gd}(t) + \lambda_i e_{iq}(t). \quad (24)$$

Assuming $\dot{S}_d(t)$ and $\dot{S}_q(t)$ equal zero and incorporating the exponential reaching law, as delineated in [7], give the following GSC switching signals

$$u_{gd}(t) = \left(R_f + R_g\right) i_{gd}(t) + e_{gd}(t) - \left(L_f + L_g\right) \left(i^*_{gd}(t) - \omega_g(t) i_{gq}(t) + \lambda_i e_{id}(t)\right) - \varepsilon_i \, sgn\left(S_d(t)\right) - k_i S_d(t). \quad (25)$$

$$u_{gq}(t) = \left(R_f + R_g\right) i_{gq}(t) + e_{gq}(t) - \left(L_f + L_g\right) \left(i^*_{gq}(t) + \omega_g(t) i_{gq}(t) + \lambda_i e_{id}(t)\right) - \varepsilon_i \, sgn\left(S_q(t)\right) - k_i S_q(t). \quad (26)$$

here, ε_i and k_i are the tuning parameters for increasing the convergence rate.

Simulation Results

To assess the efficacy of the proposed SMC approach for GSC control, computational simulations were performed within a MATLAB framework. The voltage and current controllers operate at a sampling period of $1ms$ and their tuning parameters are set as $\lambda_v = 5,\ \lambda_i = 30,\ \varepsilon_v = \varepsilon_i = 3$ and $k_v = k_i = 1$. The system parameters used in this paper are depicted in Table 1.

Table 1: System parameters.

Subsystem	Specifications		
	Parameter	***Symbol***	***Value***
Machine-side	Total mass	m	3×10^4 kg
	PMLG flux linkage	φ_{pm}	19.8 Wb
	PMLG pole pitch	τ_p	0.045 m
	PMLG impedance	R_s, L_s	2 Ω, 32 mH
	DC bus capacitor	C_{dc}	2.7 mF
	Nominal DC bus voltage	v_{dc}	2000 V
Grid-side	L filter inductance	L_f	2 mH
	L filter resistance	R_f	40 mΩ
	Grid RMS voltage (line to line)	E_{gn}	563.4 V
	Grid frequency	f_g	50 Hz
	Grid impedance	R_g, L_g	20 mΩ, 0.1 mH

Fig. 3 demonstrates the efficacy of the voltage controller in the presence of polychromatic wave of significant height 4 m and dominant frequency 0.65 rad/s. As evidenced in Fig. 3a, the DC voltage controller successfully sustained the bus voltage at its desired reference level of 2000 V. Voltage fluctuations were noted, particularly a 1.84 V increase at 87.5 s, due to P_e exceeding P_g by 8.28 kW, as shown in Fig. 3b. Throughout the simulation from 60 s to 140 s, the PA generated an average power output of 3.59 kW and delivered an average power of 3.53 kW to the electrical grid. This confirms that a majority of generated power is efficiently transferred to the grid with minor discrepancies due to switching losses.

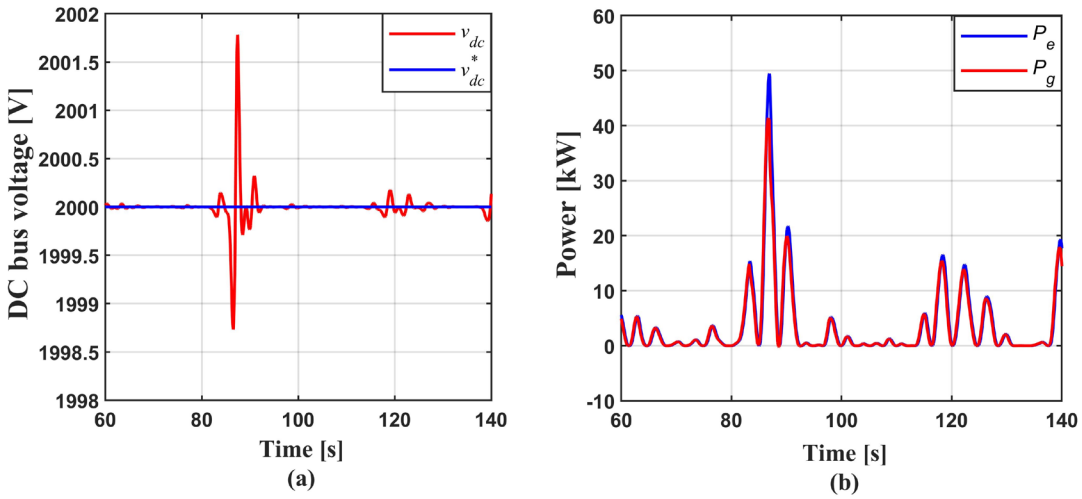

Figure 3: The voltage control loop performance: (a) DC voltage (b) power plots.

Fig. 4a and 4b show the performance of the low-level controllers for direct and quadrature currents, respectively. The direct current reference i_{gd}^* is determined by the DC voltage controller, which augments its value in response to a rise in DC voltage, thereby boosting the power injected into the electrical grid. The direct current reached a maximum peak of 86.7 A in reaction to the highest DC bus voltage at 87.5 s. The quadrature current controller managed to regulate its respective current i_{gq} to zero to ensure a unity power factor. However, minor oscillations in both positive and negative directions were observed, attributable to the coupling effects between i_{gq}

and i_{gd}, especially at peak values of i_{gd}. Fig. 5 shows the power quality at the point of common coupling, with Fig. 5a displaying the three-phase grid injected currents and Fig. 5b confirming voltage and current of Phase A are synchronized for a unity power factor.

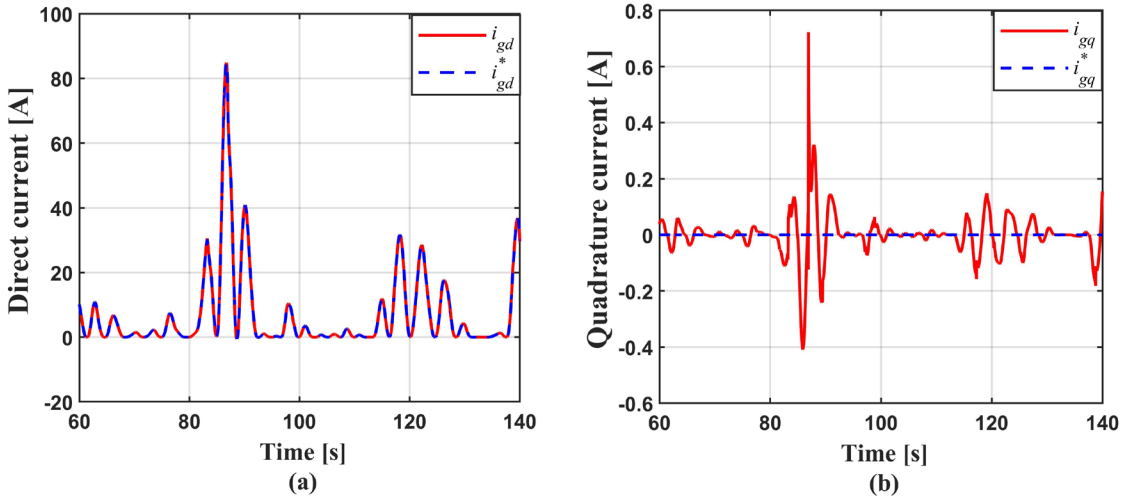

Figure 4: The current control loop performance: (a) direct current (b) quadrature current.

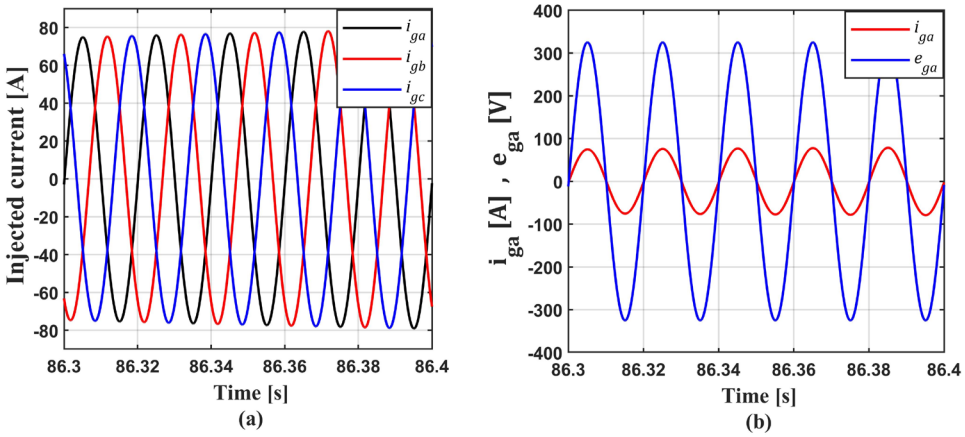

Figure 5: Power quality: (a) three phase injected current (b) grid voltage and current at phase A

Conclusion

This paper highlights the effectiveness of a sliding mode control strategy, incorporating an exponential reaching law within a voltage-oriented control architecture, for integrating a PA type WEC into the power grid. The study's primary goal was to enhance the transfer of generated power to the grid while maintaining the DC bus voltage at a set level and securing a unity power factor, addressing the inherent challenges posed by the variable nature of wave energy. Simulation outcomes, achieved through a MATLAB environment, validate the proposed control strategy's ability to maintain designated DC bus voltage levels and manage the direct and quadrature currents effectively by reducing tracking errors. This research contributes to the field by providing a robust control solution that can improve the reliability and efficiency of wave energy conversion systems when integrated into electrical grids.

References

[1] A. Wahyudie and M. Jama, "Perspective on damping control startegy for heaving wave energy converters," *IEEE Access*, vol. 5, 99. 22224-22233, 2017. https://doi.org/10.1109/ACCESS.2017.2757278

[2] O. Saeed *et al*, "Simple resonance circuit to improve power conversion in a two-sided planar permanent magnet linear generator for wave energy converters," *IEEE Access*, vol. 5, pp. 18654-18664, 2017. https://doi.org/10.1109/ACCESS.2017.2752466

[3] M. Jama *et al.*, "Self-tunable fuzzy logic controller for optimization of heaving wave energy converters," *in proc. of ICRERA 2012, pp. 6477273, 2012*. https://doi.org/10.1109/ICRERA.2012.6477273

[4] S. Rasool *et al*, "Coupled modeling and advanced control for smooth operation of a grid-connected linear electric generator based wave-to-wire system," *IEEE Transactions on Industry Applications,* vol. 56, no. 5, pp. 5575-5584, 2020. https://doi.org/10.1109/TIA.2020.3004759

[5] H. A. Said, D. García-Violini, and J. V. Ringwood, "Wave-to-grid (W2G) control of a wave energy converter," *Energy Conversion and Management: X,* vol. 14, p. 100190, 2022. https://doi.org/10.1016/j.ecmx.2022.100190

[6] K. Zeb *et al.*, "A comprehensive review on inverter topologies and control strategies for grid connected photovoltaic system," *Ren. and Sust. Energy Reviews,* vol. 94, pp. 1120-1141, 2018. https://doi.org/10.1016/j.rser.2018.06.053

[7] J. Liu, *Sliding mode control using MATLAB*. Academic Press, 2017. https://doi.org/10.1016/B978-0-12-802575-8.00005-9

[8] A. Y. Elamin *et al.*, "Real-time Model Predictive Control Framework for a Point Absorber Wave Energy Converter with Excitation Force Estimation and Prediction," *IEEE Access,* 2023. https://doi.org/10.1109/ACCESS.2023.3347731